ELSEVIER

Computer Aided Geometric Design 18 (2001) 483–502

COMPUTER AIDED GEOMETRIC DESIGN

www.elsevier.com/locate/comaid

A subdivision scheme for surfaces of revolution

Géraldine Morin, Joe Warren *, Henrik Weimer

Rice University, Department of Computer Science, Houston, TX 77251-1892, USA

Received June 2000; revised February 2001

Abstract

This paper describes a simple and efficient non-stationary subdivision scheme of order 4. This curve scheme unifies known subdivision rules for cubic B-splines, splines-in-tension and a certain class of trigonometric splines capable of reproducing circles. The curves generated by this unified subdivision scheme are $\boldsymbol{C}^2$ splines whose segments are either polynomial, hyperbolic or trigonometric functions, depending on a single tension parameter. This curve scheme easily generalizes to a surface scheme over quadrilateral meshes. The authors hypothesize that this surface scheme produces limit surfaces that are $\boldsymbol{C}^2$ continuous everywhere except at extraordinary vertices where the surfaces are $\boldsymbol{C}^1$ continuous. In the particular case where the tension parameters are all set to 1, the scheme reproduces a variant of the Catmull–Clark subdivision scheme. As an application, this scheme is used to generate surfaces of revolution from a given profile curve. © 2001 Published by Elsevier Science B.V.

1. The curve scheme

We begin by considering the three related curve schemes: cubic splines, splines-in-tension and a certain class of trigonometric splines. Based on the description of these splines in terms of their locally supported basis functions, we generate known subdivision masks for each scheme. Finally, we derive a new, common subdivision mask that unifies these three families of splines. More details on the study of these splines, their characteristic differential equation, and the links between differential equations and subdivision are given by Warren and Weimer (2001).

* Corresponding author.
E-mail addresses: gege@rice.edu (G. Morin), jwarren@rice.edu (J. Warren), henrik@rice.edu (H. Weimer).

0167-8396/01/$ – see front matter
PII: S0167-8396(01)00043-7

1.1. The underlying spline spaces

The curve subdivision scheme proposed in this section converges to piecewise functions whose segments are solutions to the differential equation

$$\boldsymbol{p}^{(4)}[\boldsymbol{x}] - \gamma\, \boldsymbol{p}^{(2)}[\boldsymbol{x}] == 0. \tag{1}$$

Depending on the sign of γ, the solutions to this differential equation can be expressed as follows:

- If $\gamma == 0$, then the solutions $\boldsymbol{p}[\boldsymbol{x}]$ to this equation are the polynomials $1, \boldsymbol{x}, \boldsymbol{x}^2, \boldsymbol{x}^3$.
- If $\gamma > 0$, then the solutions $\boldsymbol{p}[\boldsymbol{x}]$ to this equation are the functions 1, $\boldsymbol{x}$, $\cosh[\sqrt{\gamma}\,\boldsymbol{x}]$, $\sinh[\sqrt{\gamma}\,\boldsymbol{x}]$.
- If $\gamma < 0$, then the solutions $\boldsymbol{p}[\boldsymbol{x}]$ to this equation are the functions 1, $\boldsymbol{x}$, $\cos[\sqrt{-\gamma}\,\boldsymbol{x}]$, $\sin[\sqrt{-\gamma}\,\boldsymbol{x}]$.

(If $\gamma < 0$, then we assume that $\sqrt{-\gamma}\,\beta_0 < \pi$.)

Given a uniform knot sequence T_k of the form

$$\beta_k\mathbb{Z} = \{\ldots, -2\beta_k, -\beta_k, 0, \beta_k, 2\beta_k, \ldots\},$$

we can consider the space V_k of splines whose segments satisfy Eq. (1) and that are at least $\boldsymbol{C}^2$ continuous at the knots T_k. These splines are instances of a general class of splines known as L-splines (Schumaker, 1981). Due to the uniformity of the knot sequence, the space V_k can be expressed as the span of the translates of a single $\boldsymbol{C}^2$ basis function $\boldsymbol{N}_k[\boldsymbol{x}]$ that is supported on the interval $[-2\beta_k, 2\beta_k]$. (In the trigonometric case $\gamma < 0$, we restrict β_k such that $\sqrt{-\gamma}\,\beta_k < \pi$.)

Due to the fact that the function 1 is in the solution space of Eq. (1), these basis functions can be normalized such that the translates of the basis function $\boldsymbol{N}_k[\boldsymbol{x}]$ form a partition of unity, i.e.,

$$\sum_i \boldsymbol{N}_k[\boldsymbol{x} - i\beta_k] == 1. \tag{2}$$

For $\gamma == 0$, the space V_k is the space of cubic splines and the basis function $\boldsymbol{N}_k[\boldsymbol{x}]$ is the cubic B-spline basis function. For $\gamma > 0$, the space V_k is the space of splines-in-tension (Hoschek and Lasser, 1993). The parameter γ serves as a "tension" parameter that forces the resulting spline to vary between a linear and cubic spline. For $\gamma < 0$, the space V_k is a "mixed" space consisting of polynomial and trigonometric functions. This spline space has been studied previously in (Zhang, 1996) and Koch and Lyche (1991). When used parametrically, the functions of this mixed space are capable of reproducing circles.

1.2. The corresponding subdivision masks

Henceforth, we assume that the knot spacing between successive levels is related by a factor of two, i.e., $\beta_k = \frac{1}{2}\beta_{k-1}$. Since the initial knot sequence T_0 is centered at the origin, the knot sequence T_{k-1} is now a subsequence of T_k. In particular, the functions in V_{k-1} are automatically $\boldsymbol{C}^2$ at the knots of T_k. Therefore, these spaces are nested, i.e., $V_{k-1} \subset V_k$ for all k, due to the fact that their segments satisfy Eq. (1) independent of k. Thus, the

basis function $\boldsymbol{N}_{k-1}[\boldsymbol{x}]$ can be expressed as a linear combination of translates of the basis function $\boldsymbol{N}_k[\boldsymbol{x}]$. In particular, there exists a unique subdivision mask s_{k-1} such that

$$\boldsymbol{N}_{k-1}[\boldsymbol{x}] == \sum_{i=-2}^{2} s_{k-1}^i \boldsymbol{N}_k[\boldsymbol{x} - i\beta_k], \tag{3}$$

where s_{k-1}^i is the ith entry of s_{k-1}. Since the basis function $\boldsymbol{N}_{k-1}[\boldsymbol{x}]$ is supported over the interval $[-2\beta_{k-1}, 2\beta_{k-1}] == [-4\beta_k, 4\beta_k]$, the mask s_{k-1} has only five non-zero entries s_k^i corresponding to the basis functions $\boldsymbol{N}_k[\boldsymbol{x} + 2\beta_k]$, $\boldsymbol{N}_k[\boldsymbol{x} + \beta_k]$, $\boldsymbol{N}_k[\boldsymbol{x}]$, $\boldsymbol{N}_k[\boldsymbol{x} - \beta_k]$ and $\boldsymbol{N}_k[\boldsymbol{x} - 2\beta_k]$. For $\gamma == 0$, this subdivision mask, first introduced by Lane and Reisenfeld (1980), has the form

$$s_{k-1} = \frac{1}{8}(1, 4, 6, 4, 1). \tag{4}$$

For $\gamma > 0$, the subdivision mask s_{k-1} for splines-in-tension can be expressed as an exponential B-spline using imaginary exponents (Dyn and Ron, 1992). Using the definition of hyperbolic cosine cosh, this mask can be reduced to the real form:

$$s_{k-1} = \frac{1}{4 + 4\cosh[\sqrt{\gamma}\,\beta_k]}\big(1, 2 + 2\cosh\big[\sqrt{\gamma}\beta_k\big], 2 + 4\cosh\big[\sqrt{\gamma}\beta_k\big], 2 + 2\cosh\big[\sqrt{\gamma}\beta_k\big], 1\big). \tag{5}$$

Warren and Weimer (2001) give a full derivation of this mask starting from the original differential equation. Finally, for $\gamma < 0$, Zhang (1996) expresses the subdivision mask for "mixed" trigonometric splines (C-splines in his terminology) as:

$$s_{k-1} = \frac{1}{4 + 4\cos[\sqrt{-\gamma}\,\beta_k]}\big(1, 2 + 2\cos\big[\sqrt{-\gamma}\beta_k\big], 2 + 4\cos\big[\sqrt{-\gamma}\beta_k\big], 2 + 2\cos\big[\sqrt{-\gamma}\beta_k\big], 1\big). \tag{6}$$

Note that Zhang restricts the initial knot spacing β_0 to satisfy $\sqrt{-\gamma}\beta_0 < \pi$. (We will also assume this restriction.) An order 3 variant of this subdivision scheme is presented by Dyn and Levin (1999). As we shall see, Eqs. (4), (5), and (6) share enough common structure that these three separate schemes can be expressed as a single common subdivision mask.

1.3. The unified subdivision scheme

The common thread linking all three of these subdivision schemes is that they can be expressed in a single mask s_k of the form

$$s_{k-1} = \frac{1}{4 + 4\alpha_k}(1, 2 + 2\alpha_k, 2 + 4\alpha_k, 2 + 2\alpha_k, 1), \tag{7}$$

where the value of α_k depends on the sign of γ. Note that the mask s_{k-1} uses the tension parameter α_k, not α_{k-1}. The reason for this indexing choice is explained in the next section. Here we distinguish three cases, based on the sign of γ:

- If $\gamma == 0$, then $\alpha_k = 1$.

- If $\gamma > 0$, then $\alpha_k = \cosh[\sqrt{\gamma}\beta_k]$. Note that for this case $\alpha_k > 1$ for all k.
- If $\gamma < 0$, then $\alpha_k = \cos[\sqrt{-\gamma}\beta_k]$. Given the restriction that $\sqrt{-\gamma}\beta_0 < \pi$, then $\alpha_k < 1$ for all k in this case.

At first glance, this separation of α_k into three cases seems to provide little help. However, the following theorem makes these three cases unnecessary once the initial tension α_0 has been chosen.

Theorem 1. *If the knot spacing satisfies $\beta_k = \frac{1}{2}\beta_{k-1}$, then, for all three of the cases above, α_{k-1} and α_k satisfy the recurrence*

$$\alpha_k = \sqrt{\frac{1+\alpha_{k-1}}{2}} \tag{8}$$

for all $k > 0$.

Proof. In the hyperbolic case ($\gamma > 0$), the initial tension α_0 is always greater than 1 and the theorem follows directly from the hyperbolic identity $\cosh[\theta]^2 == \frac{1+\cosh[2\theta]}{2}$. In the trigonometric case ($\gamma < 0$), the restriction $\sqrt{-\gamma}\beta_0 < \pi$ implies that $\alpha_k \geqslant 0$ for $k > 0$ and the theorem follows directly from the trigonometric identity $\cos[\theta]^2 == \frac{1+\cos[2\theta]}{2}$. □

Given the tension α_{k-1}, the subdivision mask s_{k-1} is derived by first computing α_k using Eq. (8) and by then substituting α_k into Eq. (7). This non-stationary subdivision scheme combines the three previous schemes in a very elegant manner. Instead of choosing γ and β_0, the user simply chooses an initial "tension" α_0. If the initial tension is $\alpha_0 == 1$, then $\alpha_k == 1$ for all k and the subdivision scheme is the cubic B-spline subdivision algorithm of Lane and Reisenfeld. If $\alpha_0 > 1$, then the scheme converges to a spline-in-tension. As desired, larger initial tensions α_0 lead to curves that behave more like linear splines. If $-1 \leqslant \alpha_0 < 1$, then the scheme converges to a "mixed" trigonometric spline.

Fig. 1 shows the effect of varying initial tensions α_0 on the resulting splines. In particular, the figure shows a diamond-shaped polygon and the corresponding splines for $\alpha_0 = \{-1, 0, 1, 10, 100\}$. Varying α_0 control the distribution of the curvature of the spline. Larger value of α_0 causes most of the curvature to be concentrated need the vertices of the control polygon, i.e., the spline "clings" to the control polygon. Smaller values tends to distributes more of the curvature along the edges of the control polygon. At the extreme case of $\alpha_0 = -1$, almost all of the curvature occurs near the midpoints of the control polygon.

The second example from the left in this figure illustrates the main application of the trigonometric case; reproducing a circle. Setting $\gamma == -1$ yields a spline that can represent the functions $\sin[\boldsymbol{x}]$ and $\cos[\boldsymbol{x}]$ on the periodic domain $[0, 2\pi]$. Splitting this

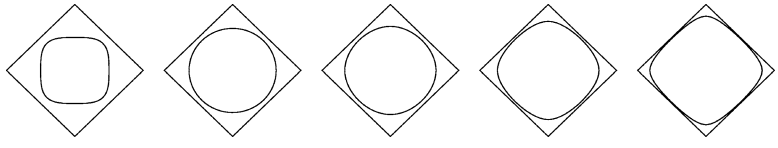

Fig. 1. The effect of varying the initial tension α_0 on the limit curve.

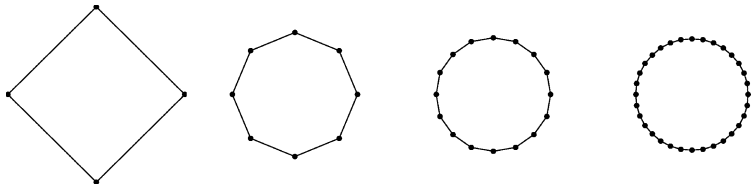

Fig. 2. Subdivision of a regular m-gon using the initial tension $\alpha_0 = \cos[2\pi/m]$ converges to a circle.

domain into m intervals by setting $\beta_0 = 2\pi/m$ yields an initial tension $\alpha_0 == \cos[2\pi/m]$. For $\gamma == -1$, we require $\beta_0 > \pi$, therefore we must take $m > 2$. Given a regular m-gon as the initial shape, the resulting scheme converges to a circle. Fig. 2 shows an example of this scheme applied to a diamond ($m == 4$).

Subdivision of a regular m-gon using the initial tension $\alpha_0 == \cos[2\pi/m]$ converges to a circle. We conclude this section by noting that the tensions α_k satisfying Eq. (8) converge to 1 as $k \to \infty$. In practice, this fact means that the subdivision mask s_{k-1} of Eq. (7) is converging to the subdivision mask for cubic B-splines as $k \to \infty$. The following theorem establishes a useful bound on this rate of convergence.

Theorem 2. *Given an initial tension $\alpha_0 \geqslant -1$ ($\alpha_0 \neq 1$), the sequence of tensions α_k satisfying Eq.* (8) *obeys, for all $k > 0$, the bound*

$$0 \leqslant \frac{1-\alpha_k}{1-\alpha_0} \leqslant \frac{1}{2^k}. \tag{9}$$

Proof. It suffices to show that $0 \leqslant \frac{1-\alpha_k}{1-\alpha_{k-1}} \leqslant \frac{1}{2}$. Define the function σ as follows

$$\sigma[\alpha] = \frac{1}{2+\sqrt{2}\sqrt{1+\alpha}}. \tag{10}$$

Given Eq. (8), it is straightforward to verify that $\sigma[\alpha_{k-1}] == \frac{1-\alpha_k}{1-\alpha_{k-1}}$ using simple algebra. For $\alpha_{k-1} \geqslant -1$, $0 \leqslant \sigma[\alpha_{k-1}] \leqslant 1/2$ and the bound holds. Given Eq. (9), then the α_k are converging to 1 as $k \to \infty$. Since $\sigma[1] == 1/4$, the bound of Eq. (9) can be tightened to c/d^k for any constant d in the range $2 \leqslant d < 4$ with the constant c depending on α_0 and d. □

2. Practical considerations for the curve scheme

Since the thrust of this paper is to develop a subdivision scheme for surfaces that is of practical interest, we next address several issues for the curve scheme that impact the surface scheme. In this section, we first reformulate the curve scheme in terms of repeated averaging. This reformulation leads directly to an analogous surfaces scheme. Next, we modify the averaging method to allow for differing tensions on distinct curve segments. Finally, we derive a simple subdivision rule for curve endpoints.

2.1. The curve scheme as repeated averaging

Eq. (3) expresses a basis function at level $k-1$, $\boldsymbol{N}_{k-1}[\boldsymbol{x}]$, as a linear combination of translates of a basis function at level k, $\boldsymbol{N}_k[\boldsymbol{x}]$. This relation can be applied to an arbitrary function in V_{k-1} as follows. Given a function $\boldsymbol{p}[\boldsymbol{x}]$ in V_{k-1}, $\boldsymbol{p}[\boldsymbol{x}]$ can be expressed as linear combination of the translates $\boldsymbol{N}_{k-1}[\boldsymbol{x} - i\beta_{k-1}]$, i.e.,

$$\boldsymbol{p}[\boldsymbol{x}] = \sum_i p_{k-1}^i \boldsymbol{N}_{k-1}[\boldsymbol{x} - i\beta_{k-1}],$$

where p_{k-1}^i denotes the ith entry of a vector of coefficients p_{k-1}. (The entries of p_{k-1} may also be points defining a closed polygon.) Substituting Eq. (3) into this relation yields that $\boldsymbol{p}[\boldsymbol{x}] = \underline{\sum} p_k^i \boldsymbol{N}_k[\boldsymbol{x} - i\beta_k]$ where the entries of the vector p_k are given by the equations

$$p_k^{2i} = \frac{1}{4+4\alpha_k}\left(p_{k-1}^{i-1} + (2+4\alpha_k)p_{k-1}^i + p_{k-1}^{i+1}\right),$$

$$p_k^{2i+1} = \frac{1}{2}\left(p_{k-1}^i + p_{k-1}^{i+1}\right).$$

These equations relating p_{k-1} to p_k can be written in matrix form as $p_k = S_{k-1}p_{k-1}$. The matrix S_{k-1} is the subdivision matrix associated with the scheme. Given an initial polygon p_0, the matrices S_{k-1} define an increasingly dense collection of polygons p_k that converge to a smooth limit curve p_∞. (In the functional case, this curve p_∞ is simply the graph of the function $\boldsymbol{p}[\boldsymbol{x}]$.) For this particular scheme, S_{k-1} is a 2-slanted matrix of the form below. For convenience, we have dropped the subscript k from α_k in the following matrices.

$$S_{k-1} = \begin{pmatrix}
\cdot & \cdot & \cdot & \cdot & \cdot & \cdot & \cdot & \cdot \\
\cdot & 0 & \frac{1}{2} & \frac{1}{2} & 0 & 0 & 0 & 0 \cdot \\
\cdot & 0 & \frac{1}{4+4\alpha} & \frac{1+2\alpha}{2+2\alpha} & \frac{1}{4+4\alpha} & 0 & 0 & 0 \cdot \\
\cdot & 0 & 0 & \frac{1}{2} & \frac{1}{2} & 0 & 0 & 0 \cdot \\
\cdot & 0 & 0 & \frac{1}{4+4\alpha} & \frac{1+2\alpha}{2+2\alpha} & \frac{1}{4+4\alpha} & 0 & 0 \cdot \\
\cdot & 0 & 0 & 0 & \frac{1}{2} & \frac{1}{2} & 0 & 0 \cdot \\
\cdot & 0 & 0 & 0 & \frac{1}{4+4\alpha} & \frac{1+2\alpha}{2+2\alpha} & \frac{1}{4+4\alpha} & 0 \cdot \\
\cdot & 0 & 0 & 0 & 0 & \frac{1}{2} & \frac{1}{2} & 0 \cdot \\
\cdot & \cdot & \cdot & \cdot & \cdot & \cdot & \cdot & \cdot
\end{pmatrix}. \tag{11}$$

The key to reformulating this scheme as repeated averaging is to observe that the subdivision matrix S_{k-1} can be factored into three separate matrices. Eq. (12) shows this factorization. (Note that only a small portion of the entire matrices is shown.) S_{k-1}, the left-hand matrix in Eq. (12), can be expressed as linear subdivision (i.e., the right-most matrix in Eq. (12)) followed by two rounds of averaging.

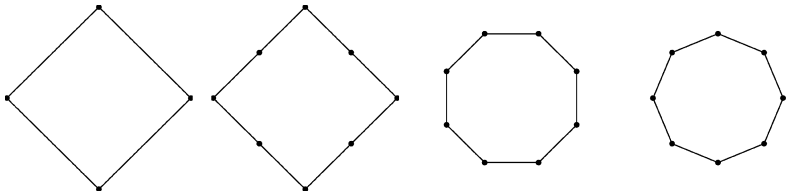

Fig. 3. One round of subdivision can be composed into the three steps linear subdivision, weighted averaging based on α_k, and midpoint averaging.

$$\begin{pmatrix} \frac{1}{4+4\alpha} & \frac{1+2\alpha}{2+2\alpha} & \frac{1}{4+4\alpha} & 0 & 0 \\ 0 & \frac{1}{2} & \frac{1}{2} & 0 & 0 \\ 0 & \frac{1}{4+4\alpha} & \frac{1+2\alpha}{2+2\alpha} & \frac{1}{4+4\alpha} & 0 \\ 0 & 0 & \frac{1}{2} & \frac{1}{2} & 0 \\ 0 & 0 & \frac{1}{4+4\alpha} & \frac{1+2\alpha}{2+2\alpha} & \frac{1}{4+4\alpha} \end{pmatrix}$$

$$== \begin{pmatrix} \frac{1}{2} & \frac{1}{2} & 0 & 0 & 0 & 0 \\ 0 & \frac{1}{2} & \frac{1}{2} & 0 & 0 & 0 \\ 0 & 0 & \frac{1}{2} & \frac{1}{2} & 0 & 0 \\ 0 & 0 & 0 & \frac{1}{2} & \frac{1}{2} & 0 \\ 0 & 0 & 0 & 0 & \frac{1}{2} & \frac{1}{2} \end{pmatrix} \cdot \begin{pmatrix} \frac{1}{1+\alpha} & \frac{\alpha}{1+\alpha} & 0 & 0 & 0 & 0 & 0 \\ 0 & \frac{\alpha}{1+\alpha} & \frac{1}{1+\alpha} & 0 & 0 & 0 & 0 \\ 0 & 0 & \frac{1}{1+\alpha} & \frac{\alpha}{1+\alpha} & 0 & 0 & 0 \\ 0 & 0 & 0 & \frac{\alpha}{1+\alpha} & \frac{1}{1+\alpha} & 0 & 0 \\ 0 & 0 & 0 & 0 & \frac{1}{1+\alpha} & \frac{\alpha}{1+\alpha} & 0 \\ 0 & 0 & 0 & 0 & 0 & \frac{\alpha}{1+\alpha} & \frac{1}{1+\alpha} \end{pmatrix} \cdot \begin{pmatrix} \frac{1}{2} & \frac{1}{2} & 0 & 0 & 0 \\ 0 & 1 & 0 & 0 & 0 \\ 0 & \frac{1}{2} & \frac{1}{2} & 0 & 0 \\ 0 & 0 & 1 & 0 & 0 \\ 0 & 0 & \frac{1}{2} & \frac{1}{2} & 0 \\ 0 & 0 & 0 & 1 & 0 \\ 0 & 0 & 0 & \frac{1}{2} & \frac{1}{2} \end{pmatrix}. \tag{12}$$

Given a coarse polygon p_{k-1}, let $\hat{p}_k$ be the new polygon produced by linear subdivision. The first round of averaging applies weighted combinations of the tension α_k to $\hat{p}_k$. This weighted averaging computes new vertices of the form $\frac{\alpha_k \hat{p}_k^i + \hat{p}_k^{i+1}}{\alpha_k+1}$ or $\frac{\hat{p}_k^i + \alpha_k \hat{p}_k^{i+1}}{\alpha_k+1}$ depending on whether i is even or odd. Most notably, this rule orients the averaging mask such that those vertices of $\hat{p}_k$ lying at vertices of p_{k-1} are weighted by $\frac{\alpha_k}{\alpha_k+1}$. Finally, the left-most matrix on the right-hand side of Eq. (12) computes a second round of averaging and places the vertices of p_k at the midpoint of these weighted averages.

For example, Fig. 3 shows the three separate transformation steps comprising the first round of subdivision in Fig. 2. The left-most polygon p_0 is a square whose initial tension is $\alpha_0 = \cos[2\pi/4] == 0$. The polygon immediately to its right, $\hat{p}_0$, is the result of applying linear subdivision. The next polygon (a stop sign) is the result of weighted averaging using the tension $\alpha_1 = \sqrt{1/2}$. Note that applying midpoint averaging here (i.e., $\alpha_1 == 1$) would not produce a regular octagon. The right-most polygon p_1 is another regular octagon that results from the final round of averaging using midpoints.

2.2. Non-uniform tensions

One standard generalization for splines-in-tension is to allow distinct values of γ for each interval of the initial knot sequence T_0. On the interior of each interval of T_0, the desired subdivision mask is exactly that of Eq. (5). However, at the knots of T_0, the subdivision mask depends the value of γ on the two neighboring intervals. One possible approach to this problem is to compute local, $\boldsymbol{C}^2$ basis functions by taking linear combinations of solutions to Eq. (1) on each interval. From these basis functions, we could then derive appropriate subdivision masks. Unfortunately, the resulting subdivision masks appear to be extremely complicated functions depending on the respective γ's and the knot spacing β_k.

A simpler alternative is to abandon the basis function approach and to simply generalize the weighted averaging rule as follows. Each segment of p_0 is assigned an initial tension α_0. During linear subdivision, each segment is split into two new segments. These new segments inherit a new tension via Eq. (8).

The resulting subdivision process is still remarkably simple. Given a vertex of p_0 sharing segments with tensions α_0 and $\hat{\alpha}_0$, respectively, the subdivision matrix S_{k-1} centered at vertex 0 is a simple modification of the matrix S_{k-1} in Eq. (12). The only modification is to replace α_k by $\hat{\alpha}_k$ in the last three rows of the weighted averaging matrix. This new non-uniform subdivision matrix S_{k-1} has the form (with subscripts k dropped),

$$
\begin{pmatrix}
\frac{1}{4+4\alpha} & \frac{1+2\alpha}{2+2\alpha} & \frac{1}{4+4\alpha} & 0 & 0 \\
0 & \frac{1}{2} & \frac{1}{2} & 0 & 0 \\
0 & \frac{1}{4+4\alpha} & 1-\frac{1}{4+4\alpha}-\frac{1}{4+4\hat{\alpha}} & \frac{1}{4+4\hat{\alpha}} & 0 \\
0 & 0 & \frac{1}{2} & \frac{1}{2} & 0 \\
0 & 0 & \frac{1}{4+4\hat{\alpha}} & \frac{1+2\hat{\alpha}}{2+2\hat{\alpha}} & \frac{1}{4+4\hat{\alpha}}
\end{pmatrix}
$$

$$
== \begin{pmatrix}
\frac{1}{2} & \frac{1}{2} & 0 & 0 & 0 & 0 \\
0 & \frac{1}{2} & \frac{1}{2} & 0 & 0 & 0 \\
0 & 0 & \frac{1}{2} & \frac{1}{2} & 0 & 0 \\
0 & 0 & 0 & \frac{1}{2} & \frac{1}{2} & 0 \\
0 & 0 & 0 & 0 & \frac{1}{2} & \frac{1}{2}
\end{pmatrix}
\cdot
\begin{pmatrix}
\frac{1}{1+\alpha} & \frac{\alpha}{1+\alpha} & 0 & 0 & 0 & 0 & 0 \\
0 & \frac{\alpha}{1+\alpha} & \frac{1}{1+\alpha} & 0 & 0 & 0 & 0 \\
0 & 0 & \frac{1}{1+\alpha} & \frac{\alpha}{1+\alpha} & 0 & 0 & 0 \\
0 & 0 & 0 & \frac{\hat{\alpha}}{1+\hat{\alpha}} & \frac{1}{1+\hat{\alpha}} & 0 & 0 \\
0 & 0 & 0 & 0 & \frac{1}{1+\hat{\alpha}} & \frac{\hat{\alpha}}{1+\hat{\alpha}} & 0 \\
0 & 0 & 0 & 0 & 0 & \frac{\hat{\alpha}}{1+\hat{\alpha}} & \frac{1}{1+\hat{\alpha}}
\end{pmatrix}
\cdot
\begin{pmatrix}
\frac{1}{2} & \frac{1}{2} & 0 & 0 & 0 \\
0 & 1 & 0 & 0 & 0 \\
0 & \frac{1}{2} & \frac{1}{2} & 0 & 0 \\
0 & 0 & 1 & 0 & 0 \\
0 & 0 & \frac{1}{2} & \frac{1}{2} & 0 \\
0 & 0 & 0 & 1 & 0 \\
0 & 0 & 0 & \frac{1}{2} & \frac{1}{2}
\end{pmatrix}
\cdot
$$

(13)

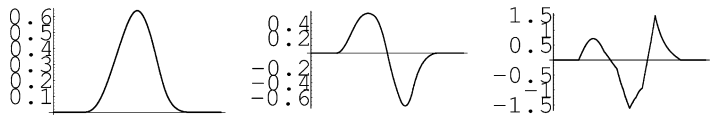

Fig. 4. A basis function with tension $\alpha_0 = 0.2$ on the left and with tension $\alpha_0 = 1.9$ on the right, together with the first and second divided differences.

Note that the resulting scheme has uniform rules everywhere except at the central vertex in question where the subdivision rule is

$$p_k^0 = \frac{1}{4+4\alpha_k} p_{k-1}^{-1} + \left(1 - \frac{1}{4+4\alpha_k} - \frac{1}{4+4\hat{\alpha}_k}\right) p_{k-1}^0 + \frac{1}{4+4\hat{\alpha}_k} p_{k-1}^1.$$

One price for abandoning the basis function approach is that we must now explicitly determine the smoothness of this new scheme at vertex 0. The left-most plot of Fig. 4 shows the basis function associated with this vertex for $\alpha_0 == 0.2$ and $\hat{\alpha}_0 == 1.9$. The middle and right plots show the first and second divided differences associated with this basis function after seven rounds of subdivision. Since the second divided differences appear to be continuous, the basis function is most likely a $\boldsymbol{C}^2$ function.

The following theorem confirms the observation that the curve scheme produces $\boldsymbol{C}^2$ limit curves.

Theorem 3. *Given a subdivision matrix S_{k-1} of the form in Eq.* (13)*, the limit curve p_∞ defined by the subdivision relation $p_k = S_{k-1} p_{k-1}$ is a $\boldsymbol{C}^2$ curve.*

Proof. See Appendix A. □

2.3. An endpoint rule

Any practical subdivision scheme for curves should include a subdivision rule for the endpoints of the curve. For our scheme, we suggest forcing interpolation at the endpoints of the curve while leaving the subdivision rules on the interior of the curve unmodified. If the endpoint has parameter value $\boldsymbol{x} == 0$, then this rule produces limit functions $\boldsymbol{p}[\boldsymbol{x}]$ that are $\boldsymbol{C}^2$ continuous at $\boldsymbol{x} == 0$ and satisfy the natural boundary condition $\boldsymbol{p}^{(2)}[0] == 0$. The reader can verify these facts by explicitly constructing the appropriately supported $\boldsymbol{C}^2$ basis functions.

This approach has the main advantage of simplicity. In particular, there is no need to modify the subdivision rules away from the endpoint. In the case of surfaces, this property avoids the complication of rules that vary as a function of their distance from the boundary and extraordinary vertices. Unfortunately, this rule also has a significant drawback. The scheme for closed curves is capable of representing circles. However, the rule for endpoints produces limit curves that are flat (i.e., have zero curvature) at the endpoints. Therefore, the proposed scheme can not represent circular arcs.

Another solution, similar to the one used by Zhang (1996) for C-curves, is to extend the control polygon by an extra segment and to use the standard, uniform rules. During each round of subdivision, the new endpoint is placed at the midpoint of the last segment, i.e.,

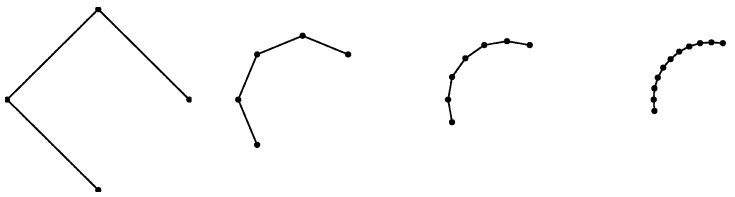

Fig. 5. Subdivision of a curve with boundary can model circular arcs.

the last segment of the refined curve is trimmed away. In our three phase implementation of the subdivision scheme, this trimming occurs automatically during the two rounds of weighted averaging after linear subdivision. If the original control polygon is chosen to be a portion of a regular n-gon, then the limit under this scheme is a circular arc. Fig. 5 shows an example of this technique used to represent a quarter circle.

As it is obvious from Fig. 5, this approach is still not an entirely satisfactory method for modeling circular arcs. An third approach is to blossom the space of solutions to Eq. (1) and to attempt to derive more general subdivision rules at the endpoint. Unfortunately, all of the authors' attempts in this direction have resulted in rules that vary on the interior of the curve and that are extremely complicated. More research remains to be done in this area.

3. The surface scheme

In the previous section, the curve scheme was expressed as linear subdivision followed by two rounds of averaging. In this section, we generalize this method to arbitrary quadrilateral surfaces. Then, as an application of the scheme, we give an algorithm for generating control polyhedra whose associated limit surfaces are surfaces of revolution. We conclude the section by performing a preliminary analysis of the smoothness of the surface scheme.

3.1. The basic scheme

A quadrilateral mesh $\{T_0, p_0\}$ (short quad mesh) consists of a topological mesh T_0 of quadrilaterals and a vector of vertex positions p_0. We propose to develop a surface subdivision scheme that is a generalization of the scheme of Catmull and Clark (1978). Given a quad mesh $\{T_{k-1}, p_{k-1}\}$, the Catmull–Clark scheme produces a new collection of quads T_k by topologically subdividing each quad in T_{k-1} into four new quads and a vector of new vertex positions p_k. These vertex positions satisfy the matrix relation $p_{k-1} = S_{k-1}p_{k-1}$ where the subdivision matrix S_{k-1} depends on the topology T_{k-1}.

Our proposed surface scheme is essentially a generalization of the curve scheme in the previous section. To perform this generalization, we must determine surface analogs for the two key components of the curve scheme: linear subdivision and weighted averaging. The analog of linear subdivision is simply bi-linear subdivision. Each quad is split into four new quads with new vertices placed at the midpoints of edges and at the centroid of each face. Given a mesh $\{T_{k-1}, p_{k-1}\}$, bi-linear subdivision produces a refined mesh $\{T_k, \hat{p}_k\}$ with the desired topology T_k.

All that remains is to determine an analog of the two rounds of averaging used to produce the final vertex positions p_k. In the curve case, the first round is a weighted averaging using the tension α_k, assigned to each edge of T_k, to compute a weighted midpoint for that edge. Recall that this tension α_k was computed via Eq. (8) from the tension α_{k-1} associated with the parent of this edge in T_{k-1}. In the surface case, we assign two tensions α_0^0 and α_0^1, one for each local coordinate direction, to each quad of T_0. Now, given a quad in T_{k-1} with tensions α_{k-1}^0 and α_{k-1}^1, each of these tensions is updated using Eq. (8) and assigned to the children of this quad in T_k during linear subdivision.

Consider a quad in T_k with indices $\binom{i_0\ i_1}{i_{10}\ i_{11}}$ where vertex i_0 is also a vertex of T_k, vertices i_1 and i_{10} lie on edges of T_{k-1} parallel to coordinate directions 0 and 1, respectively, and vertex i_{11} lies on the center of a face in T_{k-1}. (Note that the coordinate directions correspond to the superscripts of α_k^0 and α_k^1.) The centroid associated with this quad has the form

$$\text{cent} = \frac{1}{(\alpha_k^0+1)(\alpha_k^1+1)}\left(\alpha_k^0\alpha_k^1\hat{p}_k^{i_0} + \alpha_k^1\hat{p}_k^{i_1} + \alpha_k^0\hat{p}_k^{i_{10}} + \hat{p}_k^{i_{11}}\right). \tag{14}$$

In the curve case, the second round of averaging computed the midpoint of the weighted averages. For quad meshes, the first round of averaging may produce meshes that are no longer quad meshes. However, the second round of averaging always restores the topology T_k of the mesh. For non-quad meshes, this second averaging step can be viewed as simply taking the center of all of those weighted averages lying on a common face. In practice, these two averaging steps can be expressed directly as a single composite averaging rule of the form:

Weighted quad averaging. Given a vertex v of T_k, compute the centroids of those quads in T_k containing v using Eq. (14) and reposition v at the center of these points.

Fig. 6 illustrates weighted quad averaging in action. The bold lines denote the mesh $\{T_k, \hat{p}_k\}$ produced by bi-linear subdivision. To compute the new vertex position of the central black vertex, weighted quad averaging computes the gray centroids for each quad in T_k. Note that the weight $\alpha_k^0\alpha_k^1$ is always attached to the vertex of the quad that is also a vertex of T_{k-1}. Finally, the central black vertex is repositioned at the center of the gray vertices.

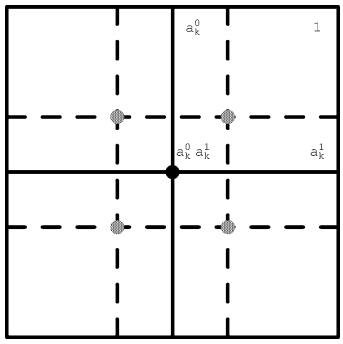

Fig. 6. Weighted quad averaging.

Note that weighted quad averaging is equivalent to two rounds of averaging in the previous sense; the first weighted, the second unweighted. Due to its simplicity, weighted quad averaging can be implemented in a very straightforward manner with a minimal amount of topological computation: Given a mesh $\{T_k, \hat{p}_k\}$ produced by bi-linear subdivision of $\{T_{k-1}, p_{k-1}\}$, first compute val$[i]$, the number of quads in T_k that contain the vertex i. This quantity can easily be computed during a single pass through T_k (or maintained during topological subdivision). Next, initialize a table of new vertex positions p_k to be all zero. Finally, make a second pass through T_k. For each quad in T_k, compute the centroid cent of its vertices in $\hat{p}_k$ using Eq. (14) and update the position of vertex i of the quad via

$$p_k^i += \frac{\text{cent}}{\text{val}[i]}. \tag{15}$$

Since there are exactly val$[i]$ quads containing vertex i, p_k^i accumulates the center of the val$[i]$ centroids.

Combing bi-linear subdivision with weighted quad averaging yields a subdivision scheme for quad meshes. In general, factoring a subdivision scheme into several simpler steps is a concept that is increasingly in popularity. For example, the idea of expressing a surface subdivision scheme in terms of repeated averaging has also appeared in two recent papers by Zorin and Schröder (2001) and Stam (2001). However, these papers use only uniform averaging and thus produce piecewise polynomial limit surfaces.

Fig. 7 shows the effect of applying this subdivision scheme to an initial quad mesh consisting of six squares forming a cube. The top row shows the effect of bi-linear subdivision. The bottom row shows the effect of weighted quad averaging, in this case with tensions $\alpha_0^0 == \alpha_0^1 == 1$ for all quads. Note that the resulting mesh has a tensor product structure everywhere except at the extraordinary points. Since bi-linear subdivision together with weighted quad averaging (with $\alpha_0^0 == \alpha_0^1 == 1$) reproduces the subdivision

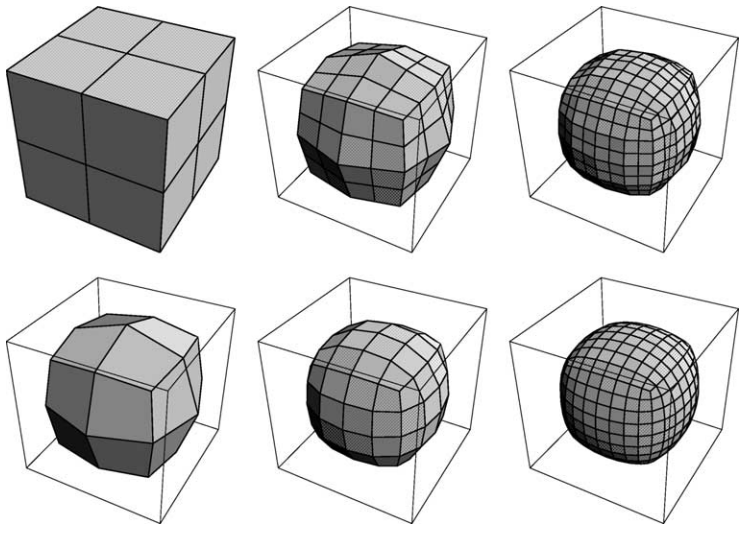

Fig. 7. Bi-linear subdivision (top row) followed by weighted quad averaging (bottom row).

rule for bi-cubic B-splines on tensor product meshes, the limit surfaces are $\boldsymbol{C}^2$ everywhere except at extraordinary points. Later in this section, we perform a more general analysis that considers the structure of the resulting subdivision rules at extraordinary vertices and examines the effect of non-uniform tensions on the smoothness of the limit surfaces.

3.2. Surfaces of revolution via the surface scheme

As a useful application of the previous scheme, we describe a simple construction for generating surface meshes whose limit surfaces are surfaces of revolution. Given a control polygon p_0 (and a list of tensions of its segments) in the $\boldsymbol{xz}$-plane, we construct a tensor product surface mesh $\{T_0, q_0\}$ (and associated tensions) in $\boldsymbol{xyz}$-space whose limit $\{T_\infty, q_\infty\}$ is the surface formed by revolving p_∞ around the $\boldsymbol{z}$-axis. We construct q_0 by making m copies of p_0 and by revolving the ith copy around the $\boldsymbol{z}$-axis by $2\pi i/m$ radians. If we decompose p_0 into its components in $\boldsymbol{x}$ and $\boldsymbol{z}$, i.e., $p_0 = (p_0^{\boldsymbol{x}}\ p_0^{\boldsymbol{z}})$, then the components of q_0 have the form

$$q_0 = \left(c\cos\left[\tfrac{2\pi i}{m}\right]p_0^{\boldsymbol{x}},\ c\sin\left[\tfrac{2\pi i}{m}\right]p_0^{\boldsymbol{x}},\ p_0^{\boldsymbol{z}}\right) \tag{16}$$

for $i = 0, \ldots, m-1$, where $c = \frac{2\pi}{m}\csc\left[\frac{2\pi}{m}\right]$.

Given that T_0 is a uniform tensor product mesh, we next assign tensions to each quad in T_0 that are compatible with the tensor product structure. Tensions α_0^0 in the direction parallel to p_0 are inherited from the tension associated with the appropriate segment of p_0. Tensions α_0^1 in the direction orthogonal to p_0 (i.e., around the $\boldsymbol{z}$-axis) are initialized to $\cos[2\pi/m]$. Consequently, cross-sections of the limit surface $\{T_\infty, q_\infty\}$ perpendicular to the $\boldsymbol{z}$-axis are circles. The constant c is chosen as to stretch $\{T_\infty, q_\infty\}$ in the $\boldsymbol{xy}$-direction and to force $\{T_\infty, q_\infty\}$ to interpolate p_∞ in the $\boldsymbol{xz}$-plane.

If $c = \frac{2\pi}{m}\csc\left[\frac{2\pi}{m}\right]$ in Eq. (16), then the limit surface $\{T_\infty, q_\infty\}$ associated with the polyhedron $\{T_0, q_0\}$ interpolates the limit curve p_∞ associated with the control polygon p_0.

Recalling the curve case, we chose $\gamma = -1$ and $\beta_0 = 2\pi/m$ to reproduce the functions cos and sin on the periodic domain $[0, 2\pi]$ split into m segments. Each basis function for this scheme was supported over four segments. For $m \geqslant 4$, the values at the three interior knots are, respectively,

$$\left\{\frac{\csc\left[\frac{\beta_0}{2}\right]^2(\beta_0 - \sin[\beta_0])}{4\beta_0}, -\frac{\csc\left[\frac{\beta_0}{2}\right]^2(\beta_0\cos[\beta_0] - \sin[\beta_0])}{2\beta_0},\right.$$
$$\left.\frac{\csc\left[\frac{\beta_0}{2}\right]^2(\beta_0 - \sin[\beta_0])}{4\beta_0}\right\}. \tag{17}$$

The key to determine c is to observe that the intersection of $\{T_\infty, q_\infty\}$ with the $\boldsymbol{xz}$-plane depends only on the portion of $\{T_0, q_0\}$ for which $i = -1, 0, 1$. Specifically, the $\boldsymbol{x}$-coordinate of $\{T_\infty, q_\infty\}$ is the linear combination of the three vectors $c * \cos[\beta_0]p_0^{\boldsymbol{x}}$, $c * p_0^{\boldsymbol{x}}$, and $c * \cos[-\beta_0]p_0^{\boldsymbol{x}}$ weighted by the corresponding values of Eq. (17). Given that we wish to reproduce $p_0^{\boldsymbol{x}}$, we can use *Mathematica* to solve for c; the result is $c = \beta_0\csc[\beta_0]$ where $\beta_0 = 2\pi/m$.

Fig. 8 shows an example of this process used to construct a vase. The upper left-most polygon is the control polygon p_0. The polygons to its right are refined polygons p_1, p_2,

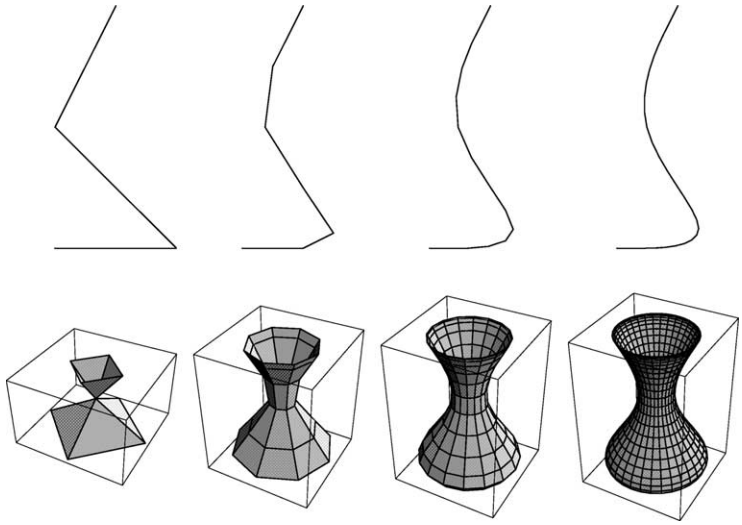

Fig. 8. Subdivision for the design of a vase.

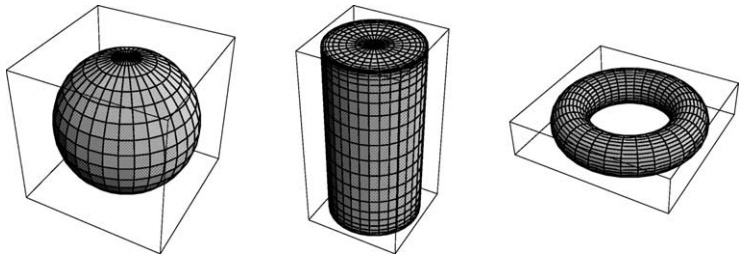

Fig. 9. A sphere, a cylinder and a torus generated via subdivision for surfaces of revolution.

and p_3. The lower left-most portion of the figure is the tensor product surface meshes q_0 formed by revolving p_0 around the z-axis. Note that a vertical cross-section of q_0 is "fatter" than p_0 due to the constant c. Subsequent meshes q_1, q_2 and q_3 appearing to the right are the result of subdivision using weighted averaging. Note that vertical cross-sections of these meshes q_k are converging to p_k.

Many fundamental surface primitives such as spheres, cylinders and tori are surfaces of revolution. Traditionally, these primitives had either been modeled as implicit surfaces or through the use of rational surface schemes. For example, Sederberg et al. (1998) describes a subdivision scheme based on an extension of NURBS that is capable of representing these primitives. However, due to the fact that the rational parameterizations for these surfaces are non-uniform, the resulting scheme cannot represent these surfaces in their natural arc-length parameterization. Fig. 9 shows a sphere, a cylinder and a torus created using our scheme. Note that the grid lines in the direction of revolution are uniformly spaced, since the scheme we propose use a uniform parameterization. (The grid lines orthogonal to the

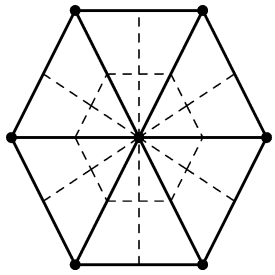

Fig. 10. Subdividing a degenerate quad mesh around a pole.

direction of revolution on the cylinder are spaced non-uniformly due to the use of repeated control points to interpolate the corners of the generating square.)

A sphere, a cylinder and a torus generated via subdivision for surfaces of revolution. In the cases of both the sphere and torus, the original profile curves p_∞ were circles. In the case of the torus, the profile curve did not intersect the z-axis and, thus, the surface of revolution was a smooth, single-sheeted surface. In the case of the sphere, the profile curve was a circle symmetrically positioned on the z-axis. Due to this positioning, the resulting surface of revolution is a smooth, *double-sheeted* surface. More generally, revolving any profile curve that is symmetric with respect to the z-axis through 2π radians results in a double-sheeted surface.

In practice, we wish to avoid this behavior when the profile curve p_∞ is symmetric with respect to the z-axis. The solution to this problem is to revolve the initial symmetric polygon p_0 through only π radians. Since the polygon p_0 is symmetric with respect to the z-axis, the new polyhedron $\bar{q}_0$ is closed (and single-sheeted). If the intersection of the z-axis and polygon p_0 occurs at vertices of p_0, then this quad mesh $\bar{q}_0$ has poles at these vertices. These poles consist of a ring of degenerate quads (triangles) surrounding the pole (as shown by the dark lines in Fig. 10).

Remarkably, applying the scheme described in the previous subsection to this polyhedron $\bar{q}_0$ yields a single-sheeted limit surface $\bar{q}_\infty$ that agrees with the double-sheeted surface of revolution q_∞. The key to this observation is to note that applying bi-linear subdivision to q_0 and $\bar{q}_0$ yield the same surface (single-sheeted and double-sheeted, respectively) as long as the degenerate quads at the poles of $\bar{q}_0$ are treated as such and subdivided as shown in Fig. 10 (the dotted lines). Weighted quad averaging also repositions the poles of $\bar{q}_0$ in the same manner as those of q_0. Thus, the limit surfaces q_∞ and $\bar{q}_\infty$ agree.

3.3. Smoothness analysis

Given a mesh $\{T_0, p_0\}$ with tensor product topology whose initial tensions obey the tensor product structure, Theorem 3 ensures that the resulting limit surfaces are $\boldsymbol{C}^2$ continuous. For example, the polyhedra $\{T_0, q_0\}$ produced by the surface of revolution algorithm have such a tensor product structure. Therefore, the associated limit surfaces $\{T_{\infty,} q_\infty\}$ are $\boldsymbol{C}^2$ continuous. However, if the tensions for each quad of T_0 are chosen without respect to this topology, then Theorem 3 is not sufficient to ensure that the limit surface is $\boldsymbol{C}^2$ continuous. In general, the authors hypothesize that, for any choice of initial tensions $\alpha_0^i \geqslant -1$, the

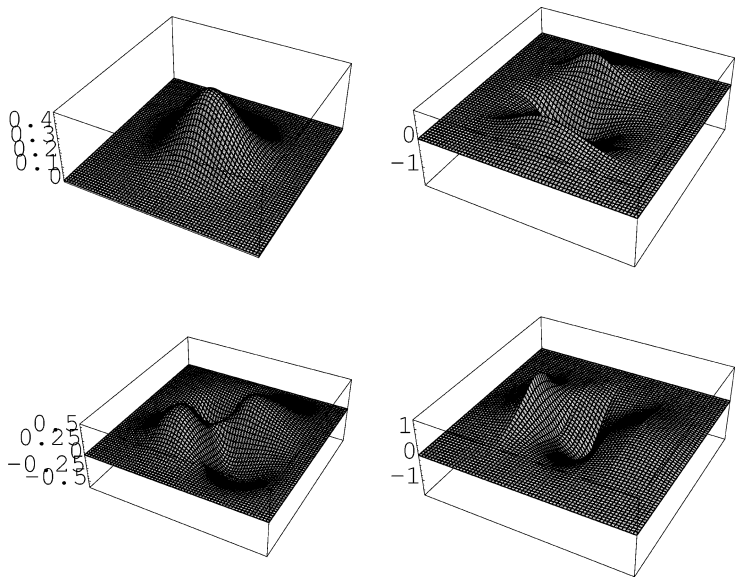

Fig. 11. A basis function for a vertex surrounded by four quads with all distinct tension parameters, together with all three possible second divided differences. The second differences appear continuous.

limit surfaces $\{T_\infty, p_\infty\}$ are $\boldsymbol{C}^2$ continuous. Specifically, we believe that a generalization of the proof for the curve case (given in Appendix A) is sufficient to establish this as a fact.

For now, we present numerical evidence that the scheme produces $\boldsymbol{C}^2$ limit surfaces on tensor product meshes. Consider a vertex surrounded by four quads with each quad assigned distinct tensions α_0^0 and α_0^1 (eight distinct tensions in all). Fig. 11 shows such a basis function and plots all three possible second divided differences. These second divided differences appear to be continuous, supporting the hypothesis that the scheme produces $\boldsymbol{C}^2$ continuous limit functions.

At extraordinary vertices, we restrict our smoothness analysis to the stationary case, i.e., $\alpha_0^0 == \alpha_0^1 == 1$. Given an extraordinary vertex of valence n, bi-linear subdivision plus quad averaging yields a subdivision rule that weights the central vertex by $\frac{9}{16}$, edge adjacent vertices by $\frac{3}{8n}$ and face adjacent vertices by $\frac{1}{16n}$. For $n == 4$, this rule reproduce the uniform rule for bi-cubic B-splines. This rule is mentioned by Catmull and Clark (1978) as an alternative to their standard rule that uses the weights $\{1 - \frac{7}{4n}, \frac{3}{2n^2}, \frac{1}{4n^2}\}$, respectively. We leave it as an exercise for the interested reader to show that the $\{\frac{9}{16}, \frac{3}{8n}, \frac{1}{16n}\}$ rule defines a subdivision matrix S_{k-1} whose spectrum has the form $1 > \lambda == \lambda > \cdots$ and whose associated characteristic map is exactly that of the standard Catmull–Clark scheme. Since the characteristic map for the standard scheme is known to be regular (see (Peters and Reif, 1998)), the stationary version of our scheme is also $\boldsymbol{C}^1$ at extraordinary vertices.

In the non-stationary case, we leave the problem of smoothness analysis at extraordinary vertices as a topic for future work. However, we observe that the rate of convergence of the non-stationary rule to the $\boldsymbol{C}^1$ stationary rule is compatible with known bounds for $\boldsymbol{C}^1$ non-

stationary schemes from the uniform case. Dyn and Levin (1992) provide the basic tools for performing such an analysis. We intend to investigate the possibility of generalizing their proof techniques to extraordinary vertices in future work.

Appendix A. A proof of C^2 continuity for the non-uniform curve scheme

In this appendix, we provide a proof for Theorem 3. Specifically, we consider the behavior of the subdivision scheme $p_k = S_{k-1}p_k$ where S_{k-1} has the form

$$\begin{pmatrix}
. & . & . & . & . & . & . \\
. & \frac{1}{4+4\alpha_k} & \frac{1+2\alpha_k}{2+2\alpha_k} & \frac{1}{4+4\alpha_k} & 0 & 0 & . \\
. & 0 & \frac{1}{2} & \frac{1}{2} & 0 & 0 & . \\
. & 0 & \frac{1}{4+4\alpha_k} & 1-\frac{1}{4+4\alpha_k}-\frac{1}{4+4\hat{\alpha}_k} & \frac{1}{4+4\hat{\alpha}_k} & 0 & . \\
. & 0 & 0 & \frac{1}{2} & \frac{1}{2} & 0 & . \\
. & 0 & 0 & \frac{1}{4+4\hat{\alpha}_k} & \frac{1+2\hat{\alpha}_k}{2+2\hat{\alpha}_k} & \frac{1}{4+4\hat{\alpha}_k} & . \\
. & . & . & . & . & . & .
\end{pmatrix}$$

with $\alpha_k = \sqrt{\frac{1+\alpha_{k-1}}{2}}$ and $\hat{\alpha}_k = \sqrt{\frac{1+\hat{\alpha}_{k-1}}{2}}$. Our goal in this appendix is to show that the limit curve p_∞ associated with this scheme is a $\boldsymbol{C}^2$ curve. Our approach is two-phased. In the first phase, we compute a subdivision matrix D_{k-1} for the divided differences associated with our original scheme. In the second phase, we show that the limit curves associated with this divided difference scheme are $\boldsymbol{C}^1$ continuous and conclude that original scheme must produce $\boldsymbol{C}^2$ limit curves.

In phase one, we follow the approach of Dyn et al. (1991) and Warren (1995). Let Δ_k be the two-banded matrix whose product $\Delta_k p_k$ is the vector consisting of the divided differences of p_k with respect to the knot sequence T_k. If D_{k-1} satisfies the matrix equation $\Delta_k.S_{k-1} = D_{k-1}.\Delta_{k-1}$, then D_{k-1} is a subdivision matrix relating the divided differences of the form $\Delta_k p_k = D_{k-1}(\Delta_{k-1}p_{k-1})$. Since S_{k-1} has rows that sum to one, the matrix D_{k-1} exists and has the form

$$D_{k-1} = \begin{pmatrix}
. & . & . & . & . & . & . & . \\
. & 0 & \frac{1+2\alpha_k}{2+2\alpha_k} & \frac{1}{2+2\alpha_k} & 0 & 0 & 0 & . \\
. & 0 & \frac{1}{2+2\alpha_k} & \frac{1+2\alpha_k}{2+2\alpha_k} & 0 & 0 & 0 & . \\
. & 0 & 0 & \frac{1+2\alpha_k}{2+2\alpha_k} & \frac{1}{2+2(\hat{\alpha})_k} & 0 & 0 & . \\
. & 0 & 0 & \frac{1}{2+2\alpha_k} & \frac{1+2(\hat{\alpha})_k}{2+2(\hat{\alpha})_k} & 0 & 0 & . \\
. & 0 & 0 & 0 & \frac{1+2(\hat{\alpha})_k}{2+2(\hat{\alpha})_k} & \frac{1}{2+2(\hat{\alpha})_k} & 0 & . \\
. & 0 & 0 & 0 & \frac{1}{2+2(\hat{\alpha})_k} & \frac{1+2(\hat{\alpha})_k}{2+2(\hat{\alpha})_k} & 0 & . \\
. & . & . & . & . & . & . & .
\end{pmatrix}.$$

Next, we analyzed the subdivision process $q_k = D_{k-1}q_{k-1}$. If the limit curves q_∞ associated with this scheme are $\boldsymbol{C}^1$, then limit curves p_∞ associated with the original subdivision process $p_k = S_{k-1}p_{k-1}$ are $\boldsymbol{C}^2$ (see the two references above for details). Ideally, we would like to repeat this process and build a divided difference scheme for D_{k-1} with respect to T_{k-1}. Unfortunately, the rows of subdivision matrix D_{k-1} do not sum to one. Therefore, such a subdivision matrix for these differences do not exist. In phase two, we use the non-stationary analysis technique of Dyn and Levin (1999, 1995). In particular, we show that the divided differences $\Delta_k q_k$ are converging to a continuous curve. Specifically, if we define $\boldsymbol{q}'_k[\boldsymbol{x}]$ to be piecewise linear function whose value at the ith knot of T_k is exact the ith entry of $\Delta_k q_k$, then we will prove that the $\boldsymbol{q}'_k[\boldsymbol{x}]$ are uniformly converging to a continuous function and therefore conclude that the limit curve q_∞ is a $\boldsymbol{C}^1$ curve.

The key to the proof is to examine the differences between $\boldsymbol{q}'_{k-1}[\boldsymbol{x}]$ and $\boldsymbol{q}'_k[\boldsymbol{x}]$. If L_{k-1} is the subdivision matrix for linear subdivision, then

$$\begin{aligned}
\left\|\boldsymbol{q}'_{k-1}[\boldsymbol{x}] - \boldsymbol{q}'_k[\boldsymbol{x}]\right\|_\infty &= \|L_{k-1}\Delta_{k-1}q_{k-1} - \Delta_k q_k\|_\infty, \\
&= \|L_{k-1}\Delta_{k-1}q_{k-1} - \Delta_k D_{k-1}q_{k-1}\|_\infty, \\
&= \left\|(L_{k-1}\Delta_{k-1} - \Delta_k D_{k-1})q_k\right\|_\infty, \\
&\leqslant \left\|(L_{k-1}\Delta_{k-1} - \Delta_k D_{k-1})\right\|_\infty \|q_{k-1}\|_\infty. \qquad (18)
\end{aligned}$$

Now, the matrix $L_{k-1}\Delta_{k-1} - \Delta_k D_{k-1}$ has a particularly simple form

$$\frac{2^k}{\beta_0}\begin{pmatrix}
. & . & . & . & . & . & . \\
. & 0 & \frac{-1+\alpha_k}{1+\alpha_k} & \frac{1-\alpha_k}{1+\alpha_k} & 0 & 0 & 0 \\
. & 0 & \frac{1-\alpha_k}{2(1+\alpha_k)} & 0 & \frac{-1+\hat{\alpha}_k}{2(1+\hat{\alpha}_k)} & 0 & 0 \\
. & 0 & 0 & \frac{-1+\alpha_k}{1+\alpha_k} & \frac{1-\hat{\alpha}_k}{1+\hat{\alpha}_k} & 0 & 0 \\
. & 0 & 0 & \frac{1-\alpha_k}{2(1+\alpha_k)} & 0 & \frac{-1+\hat{\alpha}_k}{2(1+\hat{\alpha}_k)} & 0 \\
. & 0 & 0 & 0 & \frac{-1+\hat{\alpha}_k}{1+\hat{\alpha}_k} & \frac{1-\hat{\alpha}}{1+\hat{\alpha}_k} & 0 \\
. & . & . & . & . & . & .
\end{pmatrix},$$

where β_k is the knot spacing for T_k. (Recall that $\beta_k = \frac{1}{2}\beta_{k-1}$.) Based on Theorem 2, we observe that

$$\left\|(L_{k-1}\Delta_{k-1} - \Delta_k D_{k-1})\right\|_\infty < \frac{c}{d^k}$$

for any $1 \leqslant d < 2$ with the constant c depending on α_0, $\hat{\alpha}_0$, β_0 and d. Using a similar method, one can show that, for all $k > 0$,

$$\begin{aligned}
\|q_k\|_\infty &\leqslant \left(1 + \frac{\hat{c}}{2^{k-1}}\right)\|q_{k-1}\|_\infty \leqslant \left(\prod_{i=0}^{k-1}\left(1 + \frac{\hat{c}}{2^k}\right)\right)\|q_0\|_\infty \\
&\leqslant \mathrm{e}^{2\hat{c}}\|q_0\|_\infty.
\end{aligned}$$

Substituting the bounds from the last two equations into Eq. (18) yields that

$$\left\|\boldsymbol{q}'_{k-1}[\boldsymbol{x}] - \boldsymbol{q}'_{k}[\boldsymbol{x}]\right\|_{\infty} \leqslant \frac{c * \mathrm{e}^{2\hat{c}}\|q_0\|_{\infty}}{d^k}.$$

To complete the proof, we observe that the limit function $\boldsymbol{q}'_{\infty}[\boldsymbol{x}]$ can be written as the infinite sum

$$\boldsymbol{q}'_{\infty}[\boldsymbol{x}] = \boldsymbol{q}'_{0}[\boldsymbol{x}] - \sum_{i=0}^{\infty}\left(\boldsymbol{q}'_{k-1}[\boldsymbol{x}] - \boldsymbol{q}'_{k}[\boldsymbol{x}]\right).$$

For bounded $\|q_0\|_{\infty}$, this infinite sum must converge for all $\boldsymbol{x}$ based on the ratio test applied to the previous equation. Therefore, the continuous functions $\boldsymbol{q}'_{k}[\boldsymbol{x}]$ uniformly converge to a continuous limit function $\boldsymbol{q}'_{\infty}[\boldsymbol{x}]$.

References

Catmull, E., Clark, J., 1978. Recursively generated B-spline surfaces on arbitrary topological meshes. Computer Aided Design 16 (6), 350–355.

Dyn, N., Gregory, J., Levin, D., 1991. Analysis of uniform binary subdivision schemes for curve design. Constructive Approximation 7, 127–147.

Dyn, N., Levin, D., 1999. The subdivision experience, in: Laurent, P.-J., LeMéhauté, A., Schumaker, L.L. (Eds.), Curves and Surfaces II, Academic Press, New York, pp. 229–244.

Dyn, N., Levin, D., 1992. Stationary and non-stationary binary subdivision schemes, in: Lyche, T., Schumaker, L.L. (Eds.), Mathematical Methods in Computer Aided Geometric Design, Academic Press, pp. 209–216.

Dyn, N., Levin, D., 1995. Analysis of asymptotically equivalent binary subdivision schemes. J. Math. Anal. Appl. 193, 594–621.

Dyn, N., Ron, A., 1992. Multiresolution analysis by infinitely differentiable compactly supported functions, CMS TSR #93-4. University of Wisconsin-Madison.

Hoschek, J., Lasser, D., 1993. Fundamentals of Computer Aided Geometric Design. A.K. Peters.

Koch, P.E., Lyche, T., 1991. Construction of exponential tension B-spline of arbitrary order, in: Laurent, P.-J., LeMéhauté, A., Schumaker, L.L. (Eds.), Curves and Surfaces I, Academic Press, New York, pp. 255–258.

Lane, J.M., Riesenfeld, R.F., 1980. A theoretical development for the computer generation and display of piecewise polynomial functions. Transactions on Pattern Analysis and Machine Intelligence 2 (1), 35–46.

Peters, J., Reif, U., 1998. Analysis of generalized B-spline subdivision algorithms. SIAM J. Numer. Anal. 35 (2), 728–748.

Schumaker, L.L., 1981. Spline Functions: Basic Theory. Wiley, New York.

Sederberg, T.W., Zheng, J., Sewell, D., Sabin, M., 1998. Non-uniform recursive subdivision surfaces, in: Cohen, M. (Ed.), Proceedings of SIGGRAPH 98, Computer Graphics Proceedings (July 1998, Orlando, FL), Annual Conference Series, Addison Wesley, Reading, MA, pp. 387–394.

Stam, J., 2001. On subdivision schemes generalizing uniform B-spline surfaces of arbitrary degree. Computer Aided Geometric Design 18 (5), 383–396.

Warren, J., Weimer, H., 2001. Subdivision—A Constructive Approach. Morgan Kaufmann.

Warren, J., 1995. Subdivision methods for geometric design. Unpublished manuscript, available online at http://www.cs.rice.edu/~jwarren.

Zhang, J., 1996. C-curves: An extension of cubic curves. Computer Aided Geometric Design 13, 199–217.

Zorin, D., Schröder, P., 2001. A unified framework for primal/dual quadrilateral subdivision schemes. Computer Aided Geometric Design 18 (5), 429–454.